













Promise and Peril: Stellar Contamination and Strict Limits on the Atmosphere Composition of TRAPPIST-1c from JWST NIRISS Transmission Spectra

MICHAEL RADICA ¹, CAROLINE PIAULET-GHORAYEB ¹, JAKE TAYLOR ², LOUIS-PHILIPPE COULOMBE ¹,
LOIC ALBERT ¹, ÉTIENNE ARTIGAU ^{1,3}, BJÖRN BENNEKE ¹, NICOLAS B. COWAN ^{4,5}, RENÉ DOYON ^{1,3},
DAVID LAFRENIÈRE ¹, ALEXANDRINE L'HEUREUX ¹ AND OLIVIA LIM ¹

¹*Institut Trottier de Recherche sur les Exoplanètes and Département de Physique, Université de Montréal, 1375 Avenue Thérèse-Lavoie-Roux, Montréal, QC, H2V 0B3, Canada*

²*Department of Physics, University of Oxford, Parks Rd, Oxford OX1 3PU, UK*

³*Observatoire du Mont-Mégantic, Université de Montréal, Montréal, QC H3C 3J7, Canada*

⁴*Department of Physics, McGill University, 3600 rue University, Montréal, QC, H3A 2T8, Canada*

⁵*Department of Earth and Planetary Sciences, McGill University, 3600 rue University, Montréal, QC, H3A 2T8, Canada*

(Received; Revised; Accepted)

Submitted to ApJL

ABSTRACT

Attempts to probe the atmospheres of rocky planets around M dwarfs present both promise and peril. While their favorable planet-to-star radius ratios enable searches for even thin secondary atmospheres, their high activity levels and high-energy outputs threaten atmosphere survival. Here, we present the 0.6–2.85 μm transmission spectrum of the 1.1 R_{\oplus} , ~ 340 K rocky planet TRAPPIST-1c obtained over two JWST NIRISS/SOSS transit observations. Each of the two spectra displays 100–500 ppm signatures of stellar contamination. Despite being separated by 367 days, the retrieved spot and faculae properties are consistent between the two visits, resulting in nearly identical transmission spectra. Jointly retrieving for stellar contamination and a planetary atmosphere rules out with high confidence ($>3\text{-}\sigma$) not only clear hydrogen-dominated atmospheres, but even thin, 1-bar high-mean molecular weight atmospheres rich in H_2O , NH_3 , or CO (at the $2\text{-}\sigma$ level). We find that the only atmosphere scenarios which our spectrum cannot rule out are CH_4 - or CO_2 -rich atmospheres, which are both unlikely to be retained when considering the photodestruction of CH_4 and the susceptibility of even a CO_2 -rich atmosphere to escape given the cumulative high-energy irradiation experienced by the planet. Our results further stress the importance of robustly accounting for stellar contamination when analyzing JWST observations of exo-Earths around M dwarfs, as well as the need for high-fidelity stellar models to search for the potential signals of thin secondary atmospheres.

Keywords: Exoplanets (498); Extrasolar Rocky Planets (511); Exoplanet atmospheres (487); Planetary atmospheres (1244); Low mass stars (2050)

1. INTRODUCTION

The detection and characterization of the atmospheres of rocky, Earth-sized planets is one of the key science goals of JWST. Not only is the presence of an atmosphere a top-level requirement for potential habitabil-

ity (Grenfell 2020), but constraining the composition of terrestrial planet atmospheres also has direct implications for our understanding of the formation and evolution of small planet atmospheres (Turbet et al. 2023; Krissansen-Totton & Fortney 2022; Krissansen-Totton 2023; Bolmont et al. 2017; Zahnle & Catling 2017).

In recent years, the focus of such studies has been on small planets orbiting M dwarf stars, as the small size of these late-type host stars boosts the planet's atmosphere signal, either in transmission or emission, com-

pared to Sun-like stars (e.g., De Wit et al. 2016; Wakeford et al. 2019; Kreidberg et al. 2019; Lim et al. 2023; May et al. 2023; Greene et al. 2023; Zhang et al. 2024; Kirk et al. 2024). However, the potential promise of increased atmosphere observability also comes with a corresponding peril for atmosphere retention. Late-type stars have significantly longer pre-main sequence phases than Sun-like stars, during which time, orbiting planets are subjected to large amounts of high-energy radiation (Wordsworth & Pierrehumbert 2013; Wheatley et al. 2017). Even at late times, during the M dwarf’s main sequence phase, they still maintain large outputs of high energy radiation, with L_X/L_{bol} ratios significantly higher than those of earlier-type stars (Pizzolato et al. 2003; Wright et al. 2011; Wheatley et al. 2017; Loyd et al. 2021), reaching up to $\sim 2000\times$ that of the Sun for ultra-cool M dwarfs like TRAPPIST-1 (Wheatley et al. 2017). The increased amounts of high energy radiation received by M dwarf planets results in the potential for corresponding increases in the efficiency of atmosphere loss processes (e.g., Wordsworth & Pierrehumbert 2013; Luger & Barnes 2015; Bolmont et al. 2017; Turbet et al. 2023), resulting in uncertainty as to whether rocky planets around M dwarf stars can retain atmospheres to the present day (Zahnle & Catling 2017).

Moreover, late-type stars also maintain higher levels of activity and photospheric inhomogeneities (i.e., the presence of spots and faculae) than Sun-like stars (Peacock et al. 2019; Loyd et al. 2021). Unocculted spots and faculae on the host star’s photosphere (i.e., inhomogeneities that lie outside of a planet’s transit chord), in particular, are a pernicious problem preventing the detection of M-Earth atmospheres via transit observations (Rackham et al. 2018, 2019; TRAPPIST-1 JWST Community Initiative et al. 2024). The presence of unocculted inhomogeneities, also known as the transit light source effect (TLSE), can impart spurious features in the transmission spectra of rocky planets, which can often be significantly larger than expected atmosphere features (Rackham et al. 2018, 2023; Lim et al. 2023; TRAPPIST-1 JWST Community Initiative et al. 2024). Despite these challenges, transit observations using the Hubble Space Telescope (HST) and now with JWST, have been able to widely rule out cloud-free, H/He-dominated atmospheres for rocky M dwarf planets (De Wit et al. 2016; Wakeford et al. 2019; Libby-Roberts et al. 2022; Lim et al. 2023; Lustig-Yaeger et al. 2023; Cadieux et al. 2024; Damiano et al. 2024; Kirk et al. 2024), although such extended atmospheres are already disfavoured based on mass and radius measurements alone (Agol et al. 2021). In many cases though, the TLSE, still prevents us from robustly probing sec-

ondary, or high-mean molecular weight atmospheres in transmission (e.g., Wakeford et al. 2019; Lim et al. 2023; Cadieux et al. 2024; May et al. 2023; Moran et al. 2023).

Observations of M-dwarf planets in eclipse geometry circumvent the TLSE problem but bring with them their own sets of challenges: the planet’s orbital eccentricity must be well known to calculate the phase of the eclipse, emission observations favour planets with high temperatures, potentially ruling out habitable-zone worlds, etc. Though, even without the impacts of the TLSE, emission studies of rocky M-dwarf planets, both in the JWST era and previously, have either been negative (i.e., favour atmosphereless interpretations; Kreidberg et al. 2019; Greene et al. 2023; Ih et al. 2023; Zhang et al. 2024; Mansfield et al. 2024; Xue et al. 2024) or unable to provide definitive evidence for the presence of a high-mean molecular weight atmosphere (e.g., Zieba et al. 2023).

Here, we present transit observations of TRAPPIST-1 c with JWST NIRISS/SOSS. TRAPPIST-1 c is the second innermost planet ($a=0.01580$ AU, $T_{eq}=340$ K) of the TRAPPIST-1 system, with a mass and radius of $1.3\times$ and $1.1\times$ that of the Earth, respectively (Gillon et al. 2016; Ducrot et al. 2020; Agol et al. 2021). It was first observed in transit by De Wit et al. (2016) with HST/WFC3 from $1.1 - 1.7\ \mu\text{m}$. Their observations rule out cloud-free, H/He-dominated atmosphere scenarios at $>10\text{-}\sigma$, but lack the precision to constrain the presence of a wide range (e.g., H_2O -rich, Venus-like) of higher-mean molecular weight atmospheres. TRAPPIST-1 c was then observed in emission with JWST MIRI/F1500W photometry by Zieba et al. (2023) at $15\ \mu\text{m}$. Their dayside brightness temperature of 380 ± 31 K rules out thick (>10 bar), CO_2 -rich atmospheres, but remains consistent with a thin (0.01 bar) atmosphere composed purely of CO_2 , or trace amounts of CO_2 in thinner (0.1 – 10 bar), O_2 -dominated atmospheres at a $\sim 2\sigma$ level.

This paper is organized as follows. We present the observations and data analysis in Section 2. We describe our analysis of the TLSE in Section 3, and joint modelling of the atmosphere and stellar contamination in Section 4. We then discuss our results in Section 5 and follow up with a short conclusion in Section 6.

2. OBSERVATIONS & DATA ANALYSIS

We observed two transits of TRAPPIST-1 c with the SOSS mode of JWST’s NIRISS instrument (Albert et al. 2023; Doyon et al. 2023) as part of program GO 2589 (PI: O. Lim). The first visit started at 18:37:51 UTC on October 28, 2022, and the second at 21:09:46 UTC on October 31, 2023. Each visit lasted a total of 4.6 hr,

and consisted of 159 integrations with 18 groups per integration.

2.1. Data Reduction

We reduce the time series observations (TSO) with the `exoTEDRF` pipeline¹ (Radica 2024; Feinstein et al. 2023; Radica et al. 2023), closely following standard procedures (e.g., Radica et al. 2024; Cadieux et al. 2024). We perform the correction of $1/f$ noise at the group-level (that is, before ramp fitting) using the `scale-achromatic-window` method introduced in `exoTEDRF v1.4.0`. With this algorithm, we only use rows within 30 pixels of the trace to estimate the $1/f$ level, which can potentially help to reduce residual red noise in SOSS TSOs, particularly with high group numbers (e.g., Feinstein et al. 2023; Holmberg & Madhusudhan 2023). We also perform a “piecewise” background subtraction (e.g., Lim et al. 2023; Fournier-Tondreau et al. 2024; Radica et al. 2024), whereby the standard STScI SOSS background model is scaled separately on either side of the background “step”, as we found that a single scaling for the whole detector did not adequately remove the background signal.

We extract the stellar spectrum using a simple box aperture with a width of 40 pixels, as the dilution effects due to the SOSS first and second order overlap are expected to be negligible for transit measurements (Darveau-Bernier et al. 2022; Radica et al. 2022). Finally, there are several undispersed contaminants due to background field stars (so-called “order 0” contaminants) present on the detector for both visits, several of which partially intersect the target spectral traces. These contaminants are located at wavelengths 0.670–0.675 μm , 1.642–1.658 μm , and 2.064–2.072 μm , for visit 1, and 0.975–1.001 μm , 1.251–1.279 μm , and 1.567–1.578 μm for visit 2. We simply mask these contaminants in the extracted spectra.

2.2. White Light Curve Fitting

We construct white light curves for each visit and each order by summing all flux on the detector in order 1 (0.85 – $\sim 2.8 \mu\text{m}$), and only wavelengths $< 0.85 \mu\text{m}$ in order 2. We fit these white light curves using the flexible `juliet` package (Espinoza et al. 2019). For each visit, we jointly fit the first and second order white light curves, as in Radica et al. (2024). Concretely, we fit an astrophysical transit model, as computed by `BATMAN` (Kreidberg 2015), with the orbital parameters (T_0 , the time of mid-transit, b , the orbit impact parameter, and a/R_* , the

scaled orbital semi-major axis) shared between both orders, and the scaled planet radius, R_p/R_* fit to each order individually. We, furthermore, assume a circular orbit and fix the orbital period to 2.421937 d (Agol et al. 2021). We fit, separately for each order, the two parameters of the quadratic limb darkening law, following the Kipping (2013) parameterization. We also fit a systematics model to the light curve for each order. For visit 2, the systematics model is composed of a linear trend with time, whereas for visit 1 we also include a quadratic term with time. TRAPPIST-1 is well-known to be a highly active star (Lim et al. 2023), and we, therefore, include a Gaussian process (GP) with a simple harmonic oscillator (SHO) kernel to model residual red noise in each light curve not captured by the aforementioned detrending. The SHO kernel, as implemented in `celerite` (Foreman-Mackey et al. 2017) has proven efficient at modelling the impacts of host star photospheric variations on light curves (i.e., stellar granulation, Kallinger et al. 2014; Pereira et al. 2019; Radica et al. 2024). For each visit, we fit the characteristic amplitude of the GP separately to each order but share the characteristic frequency between the two (e.g., Radica et al. 2024). Finally, we include an error inflation term for each order. Our final models therefore consist of 20 parameters for visit 1 and 18 for visit 2 — we use wide and uninformative priors in all cases.

The results of the white light curve fits are shown in Figure 1. During the pre-transit baseline of the second visit, there was a large flare event on the host star. We attempted several methods to correct this flare in the light curves e.g., detrending against the $\text{H}\alpha$ flux, computed for each integration by measuring the area between the flux in the $\text{H}\alpha$ line and a local quadratic continuum, shown in the second panels in Figure 1. However, this avenue was unsuccessful as there is a slight time delay between the appearance of the flare in the $\text{H}\alpha$ time series and in the white light curve, likely due to lags in energy release as a function of wavelength (Howard et al. 2023). We eventually decided that, since the flare occurred in the pre-transit baseline and was sufficiently separated in time from the transit itself, the optimal course of action was to simply cut the affected integration from the fit. For visit 2, we, therefore, cut the first 75 integrations of the TSO (denoted with grey shading in Figure 1).

2.3. Spectroscopic Light Curve Fitting

To construct the spectrophotometric light curves, we sum the first order flux in bins of 80 pixels (corresponding to a constant resolving power of approximately $R=25$). The combined effects of the spectrum of the

¹ <https://github.com/radicamc/exoTEDRF>, formerly known as `supreme-SPOON`.

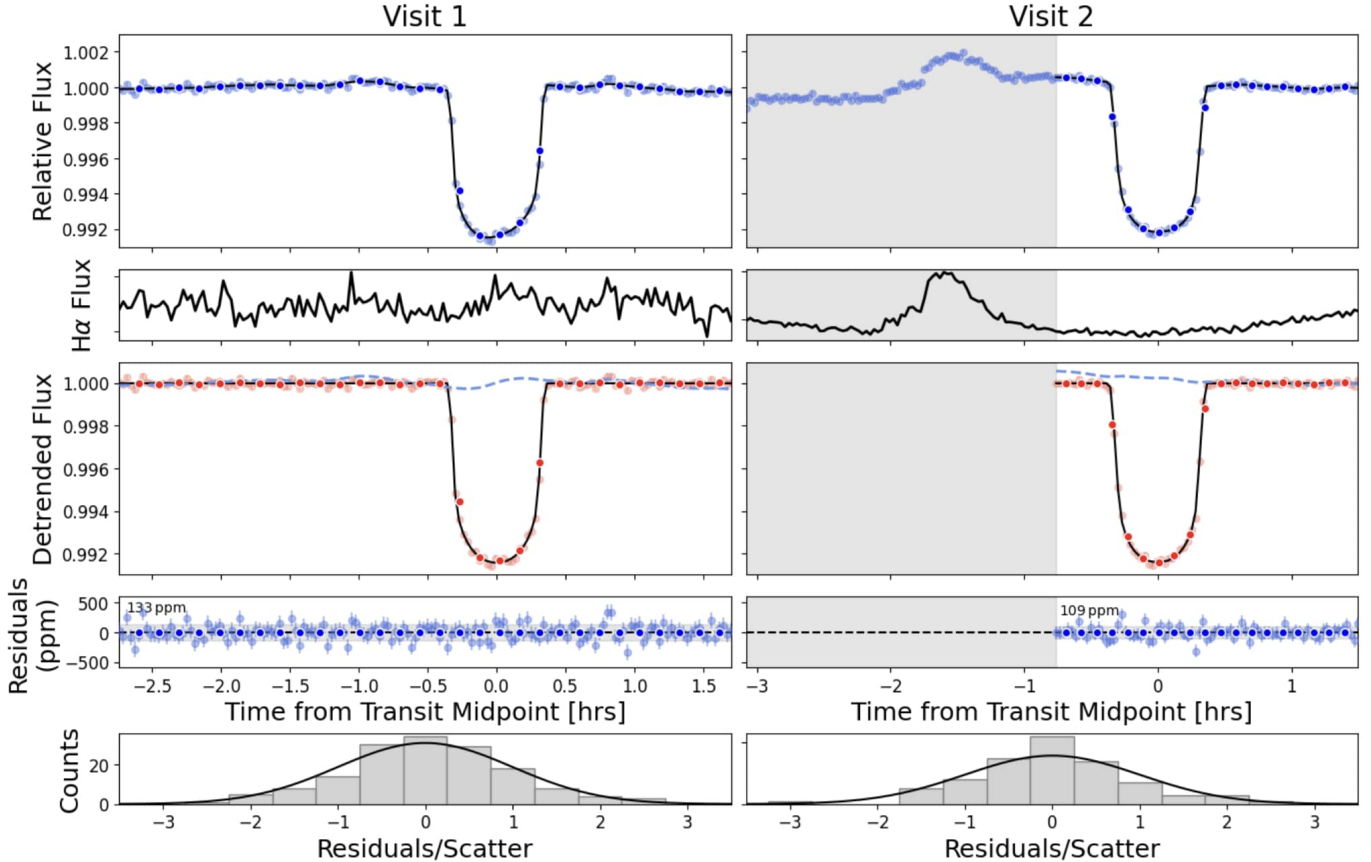


Figure 1. White light curves and fit results for both visits. *Top row:* Raw white light curves for order 1, with the best-fitting astrophysical + systematics model overplotted in black. A flare is visible in the pre-transit baseline for visit 2. The grey shading denotes integrations that were not considered in the fit. *Second row:* $H\alpha$ time series (in arbitrary units) for each visit. The time series is quiescent in visit 1, but traces the flare structure in visit 2. Note that the y-axes for both visits use different scales. *Third row:* White light curves after removal of the systematics model described in Section 2. The best-fitting astrophysical transit model is overplotted in black, and the systematics model that has been removed from the data is shown in the blue dashed line. *Fourth row:* Residuals after the removal of the astrophysical and systematics models. *Bottom row:* Histogram of residuals.

late-M host star, and the low throughput of the SOSS order 2 mean that the second order trace is incredibly faint for observations of TRAPPIST-1 planets (e.g., Lim et al. 2023). We therefore do not bin order 2 further, and simply include the white light curve results in our transit spectrum. The orbital parameters from both visits are consistent between visits (Table 1), and we therefore fix them to the weighted average between the two when fitting the spectroscopically binned light curves. We include the same systematics model as mentioned above for each visit, except that we fix the characteristic timescale of the GP to the best-fitting value from the white light fit for each visit, and allow the amplitude to freely vary, since we can reasonably expect the impacts of stellar variability to be more prominent at bluer vs. redder wavelengths (e.g., Radica et al. 2024).

We find a slight offset of ~ 122 ppm between the spectra of the two visits, which we attribute to residual

dilution from the pre-transit flare in visit 2. Indeed, this can also be noticed in the white light curve depths for each visit shown in Table 1, where the visit 2 order 1 transit depth is ~ 100 ppm shallower than visit 1 — suggestive of dilution. We tested trimming a different number of pre-transit integrations and found that this slightly changed the offset (to the tune of 5 – 10 ppm), but did not change the shape of the final transit spectrum.

We also reduce and fit the TSOs from each visit using the independent NAMELESS pipeline (Feinstein et al. 2023; Coulombe et al. 2023). Further details of this analysis are presented in Appendix A, and a comparison of the spectra from both pipelines are shown in Figure 6. Since the spectra from each pipeline are consistent to within $1\text{-}\sigma$ for both visits, we only consider the exoTDRF spectrum for the remainder of our analysis.

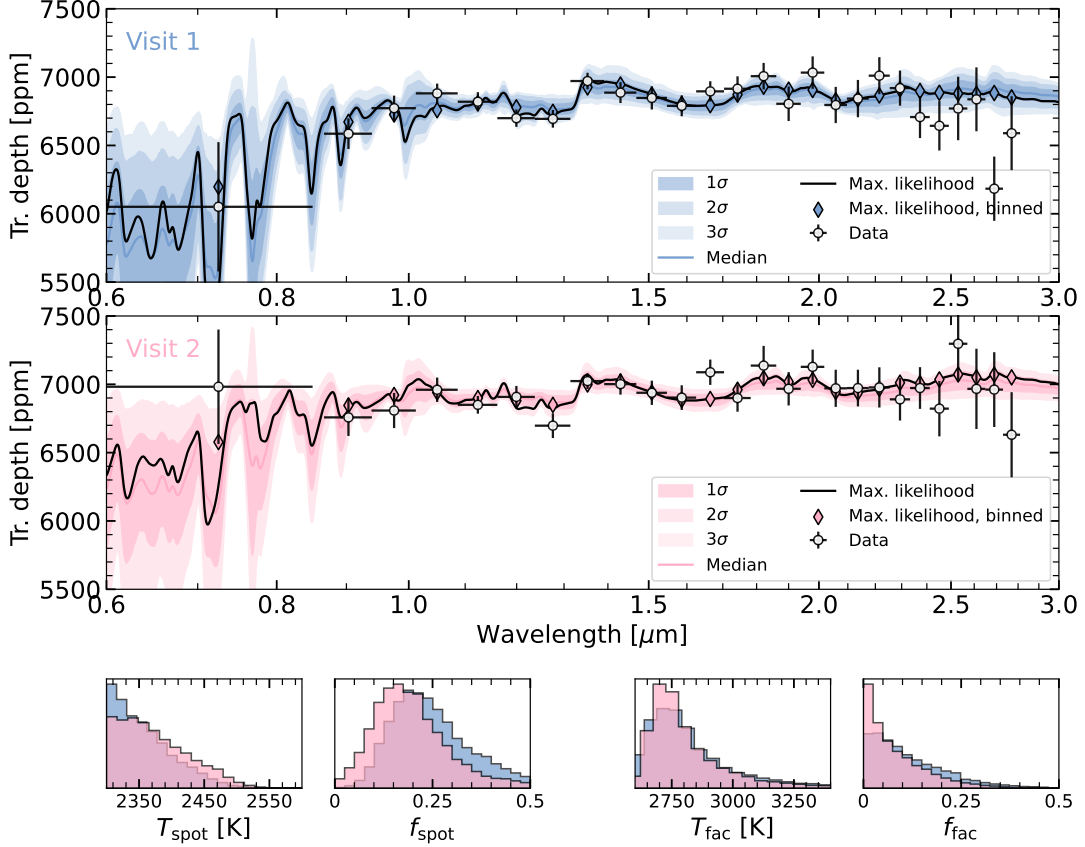


Figure 2. Results from the stellar-contamination-only fits to the transmission spectrum of each visit of TRAPPIST-1c. *Top panel:* Best-fitting unocculted heterogeneity model (black line) to the observed visit 1 spectrum (black points), and median, 1, 2, and 3- σ ranges from the posterior spectra (colour shading, smoothed to a resolving power of 100), integrated within each of the spectral wavelength bins (diamonds), for easier comparison. *Second panel:* Same as top, but for the fit to the visit 2 spectrum. *Bottom panels:* Posterior probability distributions of the spot and faculae temperatures, T_{spot} and T_{fac} , and covering fractions, f_{spot} and f_{fac} . Stellar contamination alone can explain the wavelength-dependent variations in the spectrum, and the retrieved heterogeneity parameters are largely consistent across both visits.

3. MODELLING OF THE TRANSIT LIGHT SOURCE EFFECT

We first model the transmission spectrum of TRAPPIST-1c assuming that the TLSE can completely explain each visit’s transmission spectrum. This approach is motivated by the presence of small features resembling water absorption (e.g., around $1.4\ \mu\text{m}$; Figure 2) and a pronounced slope towards short wavelengths in the spectrum of the first visit. We use the open-source code `stctm` (Piaulet-Ghorayeb 2024) to perform the TLS retrievals. We model the presence of two populations of heterogeneities: spots (covering a fraction f_{spot} of the photosphere, and cooler than the photosphere at a temperature $T_{\text{spot}} < T_{\text{phot}}$), and faculae (with f_{fac} representing their covering fraction, and $T_{\text{fac}} > T_{\text{phot}}$ their temperature).

For each population of heterogeneities, we fit for the temperature difference to the photosphere ($T_{\text{het}} = T_{\text{phot}} + \Delta T_{\text{het}}$), and place a conservative uniform prior

from 0 to 50% on the covering fraction for each of the components, f_{het} . The stellar photosphere temperature is fitted using a Gaussian prior, with the mean set by the literature value of 2566 K (Agol et al. 2021) and a standard deviation of 50 K. We allow faculae to be at most 1000 K hotter than the photosphere (with an otherwise uniform prior on $\Delta T_{\text{fac}} > 0$), while the minimum temperature of spots is set by the minimum temperature for which stellar models are available in our grid (2300 K). In the retrieval, we select at each iteration the closest-matching model (in effective temperature and surface gravity space) for the photosphere, spot, and faculae components from a finely-sampled pre-computed grid obtained with the MSG module (Townsend & Lopez 2023) using the PHOENIX (Husser et al. 2013) stellar model grid. We also fit the $\log g_{\text{het}}$ used for the heterogeneities, allowing it to be lower than that of the photosphere following recent work (Lim et al. 2023; Fournier-Tondreau

et al. 2024), but retrieve a value consistent with that of the photosphere (Agol et al. 2021).

We use the affine-invariant Markov Chain Monte Carlo sampler `emcee` (Foreman-Mackey et al. 2013) to explore the parameter space, with the number of walkers set as 20 times the number of fitted parameters, and run the chains for 5000 steps (60% are discarded as burn-in). In addition to the stellar heterogeneity properties, we fit the wavelength-independent transit depth of TRAPPIST-1 c, D . We perform independent fits to the spectrum of each visit, as they are separated by about one year and should not, a priori, be affected by the same TLS contribution. We find that similar spot and facula properties can explain both visits (Figure 2).

4. JOINT MODELLING OF ATMOSPHERE AND STELLAR CONTAMINATION

We follow up our analysis of stellar contamination by using SCARLET (Benneke & Seager 2012, 2013; Benneke 2015; Benneke et al. 2019a,b; Pelletier et al. 2021; Piaulet et al. 2023) to more thoroughly explore the potential atmosphere scenarios consistent with our observation, while still accounting for the contributions of stellar contamination. The forward modelling component of SCARLET iteratively solves the radiative transfer equation and the 1D vertical structure of the atmosphere under the assumption of hydrostatic equilibrium, given the vertical temperature-pressure profile and the molecular abundances in each atmospheric layer. In the retrieval, the planetary radius is optimized for each set of sampled parameters to obtain the best match to the observed spectrum.

We perform three categories of retrievals corresponding to different assumptions about the planetary atmosphere: (1) H_2/He -dominated scenarios; (2) single-component high-mean molecular weight atmospheres; (3) two-component high-mean molecular weight atmospheres with one infrared absorber present in the atmosphere and either N_2 or O_2 acting as the background gas.

We parameterize H_2/He -dominated atmospheres in the retrieval with a H_2/He mixture as the background gas (assuming $\text{He}/\text{H}_2 = 0.157$), log-uniform priors on the abundances of N_2 , CH_4 , H_2O , CO , CO_2 , NH_3 , and SO_2 , and a log-uniform prior on the pressure at which the atmosphere becomes opaque (either due to the presence of a cloud deck or a solid surface).

For single-component high-mean molecular weight atmospheres, we only explore absorbers with prominent features over the NIRISS/SOSS wavelength range; namely, atmospheres made of 100% CH_4 , H_2O , CO , or

NH_3 . We also fit for the “effective surface pressure” at which the atmosphere becomes opaque.

Finally, we also explore potential N_2 -dominated atmospheres (similar to some terrestrial objects in the solar system), or O_2 -dominated atmospheres (motivated by the possible $\text{O}_2\text{-CO}_2$ atmosphere consistent with the MIRI eclipse observations of TRAPPIST-1 c; (Zieba et al. 2023)) where only one of CH_4 , H_2O , CO , or NH_3 acts as an absorber, beyond the broad $\text{N}_2\text{-N}_2$ or $\text{O}_2\text{-O}_2$ collision-induced absorption features introduced by the background gas. In this retrieval setup, we fit for the partial pressure of each component.

We assume that the vertical temperature structure is isothermal, motivated by the likely-thin region of the upper atmosphere probed by our observations in transmission, and only fit for this photosphere temperature. We use the nested sampling method (Skilling 2004, 2006) to sample the full parameter space, with the multi-ellipsoid method implemented using the `nestle` module² within the SCARLET retrieval framework. The final posterior distributions are obtained from retrievals performed using at least 1000 live points. We compute forward models at $R=15,625$ before convolving them to the resolution of the data assuming a uniform throughput within each bin for the likelihood calculation.

We also calculate forward models for 1 and $100\times$ solar metallicity, H_2/He -dominated atmospheres with varying cloud-top pressures (Figure 3; left panel), and models for several high mean molecular weight compositions (Figure 4; top panel), to put our retrieval results in context. For each model, the temperature-pressure profile is assumed to be isothermal at the equilibrium temperature of TRAPPIST-1 c.

For each set of retrievals, we account in the modelling for the fact that the transmission spectra we observe are likely heavily affected by stellar contamination (see Figure 2), thereby marginalizing over the interplay that unocculted stellar heterogeneities can have with planetary absorption features. In addition to the planetary atmosphere properties, we thus account for stellar heterogeneities assuming a single population of spots, fitting for the spot covering fraction and their temperature contrast with the photosphere, as well as the photosphere temperature itself. We also assume that the stellar heterogeneity components of both visits are identical, motivated by the results from the `stctm` fit (Figure 2), and do not fit for a different $\log g$ for the heterogeneity component. We note, though, that we performed one set of atmosphere+stellar contamination retrievals where we

² <https://github.com/kbarbary/nestle>

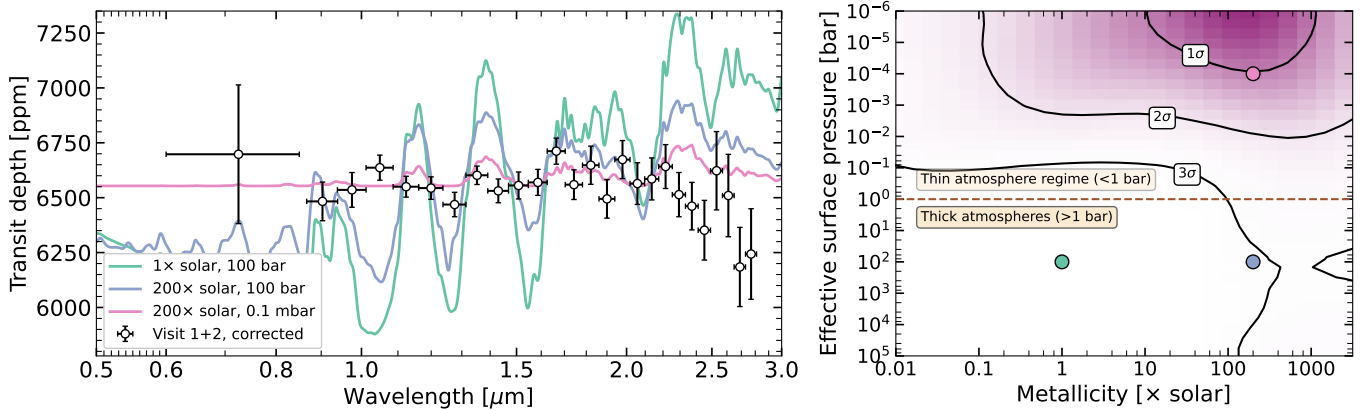


Figure 3. Constraints on H_2/He -dominated atmospheres on TRAPPIST-1c from joint atmosphere and TLSE modelling. *Left panel:* Joint visit 1+2 spectrum, corrected by the best-fitting stellar contamination model (black points), with three representative atmosphere forward models overplotted. *Right panel:* Joint posterior probability on the effective surface pressure of a H_2/He -dominated atmosphere and its metallicity from the SCARLET atmosphere retrievals (colour shading). We show the 1, 2, and 3 σ confidence regions and three markers corresponding to the three models shown in the left panel. At low metallicities, we obtain a strict 2- σ upper limit of ~ 1 mbar on any H_2/He -dominated atmosphere, although thicker (up to 0.1 bar) low-metallicity atmospheres, and thick, high-metallicity atmospheres ($>100\times$ solar) are possible within the 3 σ contours.

fit for visit-specific stellar heterogeneity properties, and found that this does not affect our inferences, further motivating our choice of shared spot parameters for both visits. We place uniform priors on the spot fraction and temperature, but use the same Gaussian prior as in the TLS-only fit for the photosphere temperature.

We note that we find a vertical offset of ~ 100 ppm between the spectra of both visits (as can be inferred from the white light transit radii presented in Table 1). We attribute it to the presence of the flare in the pre-transit baseline of the second visit that may result in a dilution effect when fitting the transit light curves and therefore fit for a parameter describing the visit 1-visit 2 offset.

5. DISCUSSION

5.1. Impacts of Stellar Contamination

Our two-transit study of TRAPPIST-1c aptly summarizes the promise and peril of transmission observations of rocky planets around M dwarf host stars. There are now a plethora of studies that have shown that stellar contamination is a true bottleneck in the attempt to detect atmospheres around rocky, M dwarf planets via transmission spectroscopy (e.g., May et al. 2023; Moran et al. 2023; Lim et al. 2023; Cadieux et al. 2024). In most cases, different manifestations of the TLSE (i.e., different temperature distributions, covering fractions, etc. of stellar spots and faculae) give rise to obviously different transmission spectra between visits, allowing for a clear inference of the impacts of the TLSE, even without undertaking in-depth modelling. Consistency in the location and shapes of spectral features between

visits has been argued to lend credence to an interpretation favouring a planetary atmosphere origin (e.g. May et al. 2023).

However, despite the high level of consistency between the transmission spectra ($\sim 1.1\text{-}\sigma$ on average), our retrieval analysis still finds that both visits can be entirely explained by stellar contamination. As shown in Figure 2, we find very similar stellar heterogeneity parameters (spot/faculae temperatures and covering fractions) for both visits. The spot and faculae temperatures are consistent with those found by Lim et al. (2023) in their analysis of NIRISS/SOSS transmission spectra of TRAPPIST-1 b. However, we find both visits to be spot-dominated, with minimal contributions from faculae, whereas Lim et al. (2023) have one spot-dominated, and one facula-dominated visit.

The consistency between visits would perhaps be unsurprising if they were separated by a very small period of time, which would therefore probe similar spot and facula distributions on the host star. However, our two visits are separated by ~ 367 d, significantly longer than the 3.3 d stellar rotation period (Luger et al. 2017). When phase-folded to the stellar rotation period, this corresponds to a phase difference of ~ 0.21 — similar to the observations of Lim et al. (2023), who, as mentioned above, found no such consistency between their two visits. This highlights the fact that TLSE models are generally non-predictive of future stellar contamination, since the distributions of spots and faculae in the host star’s photosphere is entirely stochastic (Rackham et al. 2018, 2023; TRAPPIST-1 JWST Community Initiative et al. 2024).

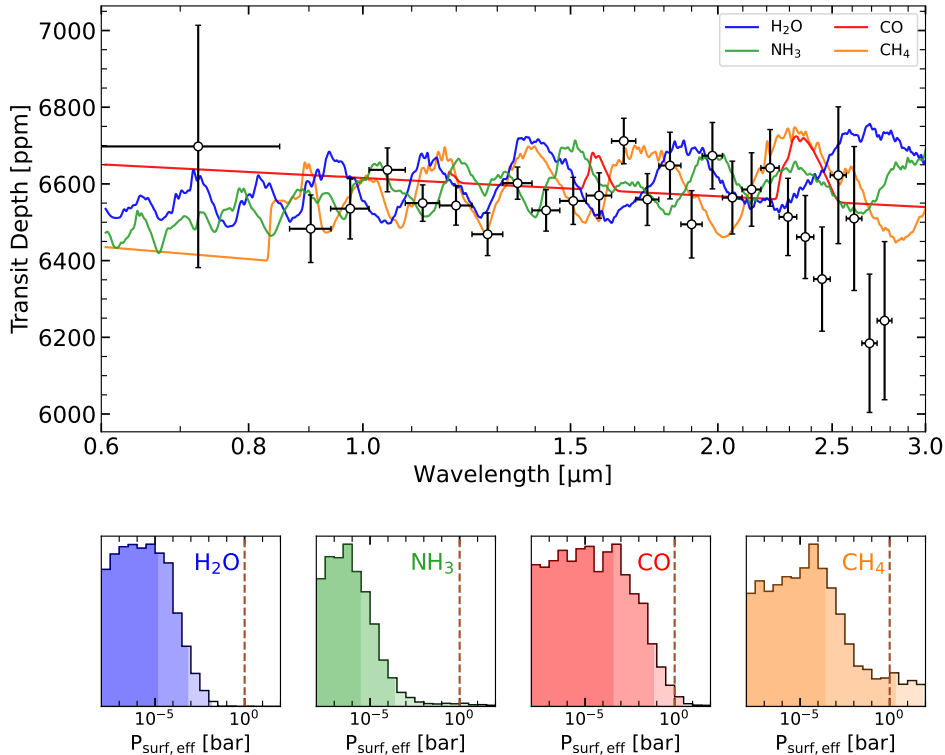


Figure 4. Constraints on high mean molecular weight atmosphere compositions for TRAPPIST-1 c. *Top panel:* Combined visit 1+2 spectrum of TRAPPIST-1 c corrected by the best-fitting stellar contamination model (black points), and atmosphere models for deep 100 bar atmospheres composed of 100% H₂O (blue), NH₃ (green), CO (red), and CH₄ (orange). *Bottom panels:* Marginalized posterior distributions on the effective surface pressure for different atmosphere compositions (labelled, with colours corresponding to the models in the top panel) The shaded areas correspond to the 1, 2, and 3 σ upper limits obtained on the effective surface pressure in each composition scenario. 1-bar atmospheres (indicated by the dashed vertical lines) are ruled out at better than 2- σ for H₂O, NH₃, and CO-rich compositions.

5.2. Cloud-Free and Thick Hydrogen-Rich Atmospheres Are Ruled Out

We find that, similarly to the closer-in planet TRAPPIST-1 b (Lim et al. 2023), we can confidently rule out thick or cloud-free hydrogen-dominated atmospheres, with a 3- σ upper limit of only 0.1 bar on the effective surface pressure of a H₂/He-dominated atmosphere atop TRAPPIST-1 c (Figure 3). The thin <0.1 bar hydrogen-rich atmosphere scenarios allowed by the transmission spectrum are, moreover, unlikely from an atmospheric evolution standpoint — TRAPPIST-1 c was exposed to large cumulative amounts of high-energy XUV irradiation from its host star, sufficient to strip away any primordial atmosphere (Hori & Ogihara 2020; Turbet et al. 2020) even when considering hydrogen outgassing (Hu et al. 2023). The transmission spectrum still allows within the 3- σ confidence contours for thick, high-metallicity (>100 \times solar) atmospheres, which may be more resilient against escape due to their higher mean molecular weights.

5.3. Limits on High Mean Molecular Weight Atmospheres

We, therefore, turn to evaluate the range of plausible high-metallicity atmosphere scenarios for TRAPPIST-1 c, and focus on the detectability of H₂O-, NH₃-, CO- and CH₄-rich atmospheres, as these infrared absorbers have sufficient opacity within the NIRISS/SOSS wavelength range to obtain meaningful constraints. We can rule out thick (>1 bar) 100% H₂O and NH₃ atmospheres at better than 3 σ , and even a 1 bar 100% CO atmosphere is excluded at the 2- σ level, although thinner \sim 0.1 bar atmospheres remain plausible explanations for the flat spectrum (Figure 4).

With the exception of CH₄, we find tight upper limits on the abundance of all the other molecules tested (H₂O, NH₃, CO), even in lower-mean molecular weight atmospheres dominated by N₂ or O₂ as the background gas (Figure 5). We compare those limits, where available, with measured compositions of solar system planets. In particular, we highlight in Figure 5 the amount of H₂O in Earth’s N₂-dominated atmosphere (using 0.4% as the mean mole fraction over the entire 1-bar atmosphere,

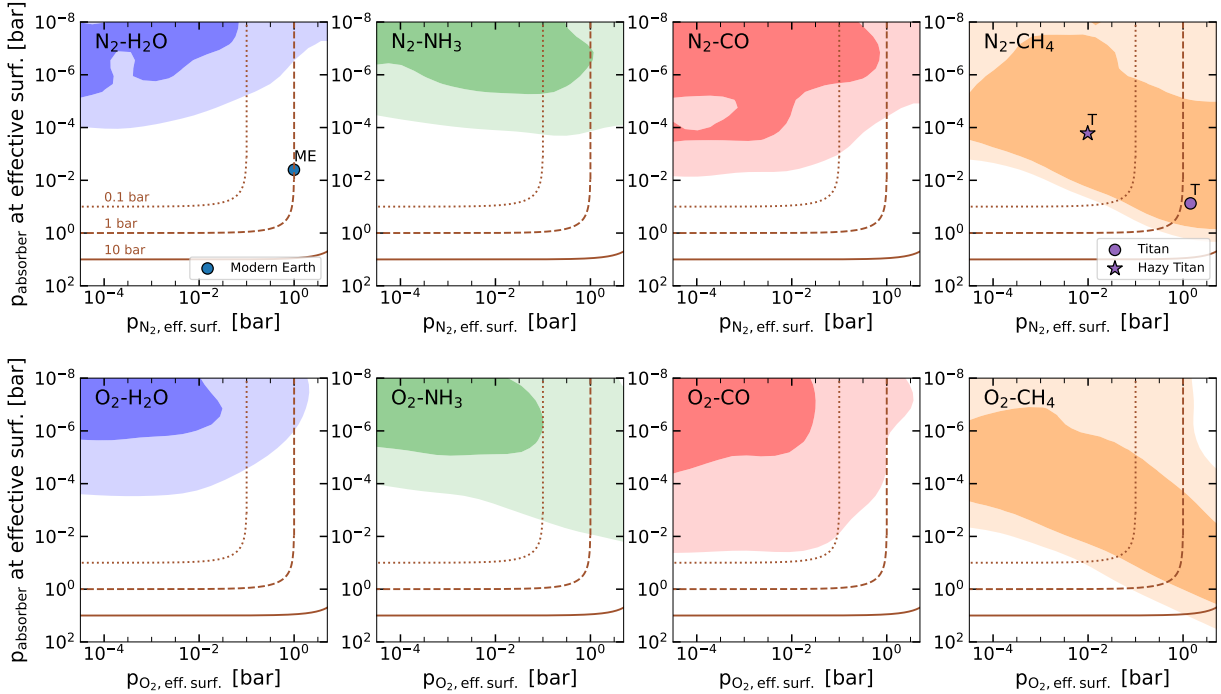


Figure 5. Constraints on N_2 - and O_2 -dominated atmospheres from the transmission spectrum of TRAPPIST-1 c. *Top panels:* Two-dimensional posterior distribution of the partial pressure of the considered absorber at the effective surface pressure (left to right: H_2O , NH_3 , CO , CH_4) as a function of the partial pressure of the background gas N_2 at the effective surface probed by the transmission spectrum. The 1 and 2σ contours are filled with different colour shadings. The parts of the parameter space corresponding to effective surface pressures of 0.1, 1, and 10 bar are outlined by the dotted, dashed, and solid sienna lines. We also illustrate where the amounts of methane in the atmosphere of Titan (with or without aerosols, purple markers; Charnay et al. 2014) and of water in the atmosphere of Modern Earth (blue marker; Kasai et al. 2011; Kelsey et al. 2022) would lie relative to our posterior distributions. *Bottom panels:* Same as the top panels, but for the retrievals with O_2 rather than N_2 as the background gas.

although it can reach about one percent at sea level; Kasai et al. 2011; Kelsey et al. 2022), or the amount of CH_4 in Titan’s atmosphere, assuming either a cloud-free Titan scenario (where one can see down to the surface) with 5% CH_4 , or a hazy scenario accounting for the fact that hydrocarbon haze opacity raises the effective surface pressure to ~ 10 mbar, and with a factor of three less methane in the upper atmosphere (see e.g. Charnay et al. 2014). We find that similar amounts of water to what is observed in Earth’s atmosphere are ruled out for TRAPPIST-1 c, while the transmission spectrum alone is not sensitive enough to the CH_4 abundance to offer meaningful constraints on Titan-like atmospheres. Although our observations cannot rule out the presence of CH_4 either in thick 1–100 bar pure- CH_4 atmospheres, or as a trace species in a N_2 - or O_2 -dominated atmosphere, CH_4 is unlikely on TRAPPIST-1 c from a modelling standpoint because of its vulnerability to destruction via photochemistry (Turbet et al. 2018).

Since O_2 is a heavier molecule than N_2 , the O_2 background scenarios generally correspond to more compact, higher mean molecular weight atmospheres. Therefore,

although the results are qualitatively similar to the N_2 -background constraints, our transmission spectrum allows for larger amounts of the tested molecular absorbers in an O_2 -dominated atmosphere. As such, we unfortunately are not able to rule on any of the possible scenarios presented by Zieba et al. (2023) based on their MIRI eclipse observations of this planet. The photometric eclipse depth of 421 ± 94 ppm at $15 \mu m$ was broadly consistent (better than 2σ) with a 0.01 bar pure CO_2 atmosphere, or trace amounts of CO_2 in a O_2 -dominated atmospheres with a surface pressure less than ~ 10 bar. We find that such an O_2 - CO_2 atmosphere would give rise in transmission to a ~ 40 ppm CO_2 absorption feature at $2.7 \mu m$ (at the red edge of the SOSS detector), and a larger ~ 90 ppm absorption band at $4.3 \mu m$. As demonstrated by Taylor et al. (2023), CO_2 cannot be reliably probed at $2.7 \mu m$ with SOSS alone, even for a hot-Jupiter, whereas the $4.3 \mu m$ feature could potentially be detectable with \sim five transits with NIRSpec/G395M or PRISM.

5.4. Implications for the Presence of an Atmosphere on TRAPPIST-1c

Ultimately, our results from the analysis of the observed transmission spectrum of TRAPPIST-1c are in line with modeling predictions that it would not have been able to retain any substantial atmosphere over the 5–9 Gyr lifetime of its host star (Burgasser & Majek 2017), regardless of its initial volatile content (Krissansen-Totton 2023).

The thin, $\lesssim 1$ bar atmospheres that remain allowed by our observations, even if they correspond to high mean molecular weights, are unlikely to be retained on TRAPPIST-1c from a theoretical perspective. Even if Jeans escape (generally less efficient than blow-off) is expected to dominate for high-mean molecular weight atmospheres atop TRAPPIST-1c, the escape rates even for resilient N_2 - CO_2 atmospheres range from one Earth atmosphere per Myr to one Earth atmosphere mass per Gyr (Van Looveren et al. 2024) at the present-day irradiation of this planet. The implications are even stricter when considering the fact that any atmosphere on TRAPPIST-1c also would have had to withstand the early XUV-active stages of the late M dwarf’s evolution (Bolmont et al. 2017), and its position inside of the runaway greenhouse limit (Turbet et al. 2020) indicates that water could not have been efficiently shielded from escape via condensation in a liquid water ocean, even if this limit is pushed to closer host star-planet distances around M dwarfs in 3D models (Turbet et al. 2023).

6. CONCLUSIONS

Here, we presented the first JWST transmission spectrum of the second innermost planet in the TRAPPIST-1 system; TRAPPIST-1c. Our 0.6 – 2.85 μm NIRISS/SOSS spectrum reveals strong contamination by the TLSE in both visits. However, unlike in previous multi-visit analyses of rocky planets around M dwarfs (e.g., May et al. 2023; Moran et al. 2023; Cadieux et al. 2024), including TRAPPIST-1b (Lim et al. 2023), we find consistent stellar heterogeneity properties between our two visits, resulting in nearly identical manifestations of the TLSE. Our results support the need for joint modelling of the TLSE and atmosphere properties to achieve robust constraints on rocky, M dwarf planets in the era of JWST. Importantly, further stellar model fidelity is critically required to accurately model out the impact of the TLSE and reach the sensitivity to detect or rule out thin atmospheres on small planets via their transit spectra.

When accounting for stellar contamination in our atmosphere analysis, we find that thick, clear hydrogen-dominated compositions are ruled out at better than

$3\text{-}\sigma$ significance, and even high-mean molecular weight compositions rich in H_2O , NH_3 or CO are excluded for an atmosphere thickness of 1 bar or more at better than 2σ . The NIRISS/SOSS transmission spectrum of TRAPPIST-1c alone cannot rule out all high mean molecular weight compositions, especially for CH_4 - and CO_2 -rich cases, to which our spectrum is not highly sensitive. However, in light of modelling predictions that CH_4 -rich compositions are unlikely as CH_4 is sensitive to photochemical destruction (Turbet et al. 2018), and considering that Jeans escape would quickly strip TRAPPIST-1c of even CO_2 -rich atmospheres (Van Looveren et al. 2024), we conclude that this planet is unlikely to bear any atmosphere whatsoever.

Regardless, as shown by Krissansen-Totton (2023), even if TRAPPIST-1c is completely atmosphere-less, this does not imply a similar fate for the outer, habitable-zone planets. Our work, though, does highlight the fact that we cannot simply rely on consistency of transmission spectra between different visits to infer the presence of a planetary atmosphere and rule out stellar contamination.

M.R. would like to acknowledge funding from the Natural Sciences and Research Council of Canada (NSERC), as well as from the Fonds de Recherche du Quebec Nature et Technologies (FRQNT). C.P.-G. acknowledges support from the NSERC Vanier scholarship, and the Trottier Family Foundation. J.T. was supported by the Glasstone Benefaction, University of Oxford (Violette and Samuel Glasstone Research Fellowships in Science 2024). A.L.H. acknowledges support from the FRQNT under file #349961. O.L. acknowledges financial support from the FRQNT. The authors acknowledge the financial support of the FRQNT through the *Centre de recherche en astrophysique du Québec* as well as the support from the Trottier Family Foundation and the Trottier Institute for Research on Exoplanets. This work is based on observations made with the NASA/ESA/CSA JWST. The data were obtained from the Mikulski Archive for Space Telescopes at the Space Telescope Science Institute, which is operated by the Association of Universities for Research in Astronomy, Inc., under NASA contract NAS 5-03127 for JWST. The specific observations analyzed can be accessed via [10.17909/ys1r-b952](https://doi.org/10.17909/ys1r-b952). This research has made use of the NASA Exoplanet Archive, which is operated by the California Institute of Technology, under contract with the National Aeronautics and Space Administration under the Exoplanet Exploration Program.

Facilities: JWST(NIRISS), Exoplanet Archive

Software: `astropy` (Astropy Collaboration et al. 2013, 2018), `celerite` (Foreman-Mackey et al. 2017),

`exoTEDRF` (Radica 2024), `exoUPRF` (Radica 2024), `ipython` (Pérez & Granger 2007), `juliet` (Espinoza et al. 2019), `jwst` (Bushouse et al. 2022), `matplotlib` (Hunter 2007), `numpy` (Harris et al. 2020), `pymultinest` (Buchner 2016), `scipy` (Virtanen et al. 2020)

APPENDIX

A. NAMELESS REDUCTION AND EXOTEP LIGHT CURVE FITTING

We reduce our two JWST NIRISS/SOSS visits of TRAPPIST-1c, starting from the uncalibrated raw data up to the extraction of the stellar spectra, using the NAMELESS pipeline (Coulombe et al. 2023; Feinstein et al. 2023). We first go through the Stages 1 and 2 steps of the STScI `jwst` pipeline (v1.12.5) (Bushouse et al. 2022), which include super-bias subtraction, reference pixel correction, non-linearity correction, ramp-fitting, and flat-fielding. We then proceed with a sequence of custom steps to correct for remaining sources of noise such as bad pixels, non-uniform background, cosmic-rays, and $1/f$ following the methods described in Benneke et al. (2024). We flag bad pixels by looking for pixels whose second derivative are significant outliers in the spatial domain. The counts of all flagged pixels are then corrected using the bicubic interpolation method of the `scipy.interpolate.griddata` function. We correct for the non-uniform background by individually scaling the two regions of the STScI model background³ that are separated by the sudden jump in background flux situated around spectral pixel $x \sim 700$. Any remaining cosmic rays are corrected by clipping any count that is more than four standard deviations away from the running median for all pixels. As for the $1/f$ noise correction, we follow the same method described in Coulombe et al. (2023) and Benneke et al. (2024) where we scale individually each column of the first and second spectral orders considering only pixels that are within a 30-pixel distance from the center of the traces to compute the $1/f$ noise. We then extract the stellar spectra from both spectral orders using a simple box aperture with a width of 36 pixels.

We perform the broadband and spectroscopic fits of the light curves produced by the NAMELESS reduction with the ExoTEP framework (Benneke et al. 2019a,b). For our fit of the white-light curve, which is obtained by summing all wavelengths of the first spectral order (0.85–2.85 μm), we keep free the mid-transit time (T_0 , considering uniform priors spanning the time of the observations for each visit), planet-to-star radius ratio (R_p/R_* , $\mathcal{U}[0.01,0.2]$), semi-major axis (a/R_* , $\mathcal{U}[15,45]$), and the impact parameter (b , $\mathcal{U}[0,1]$). We consider the quadratic limb-darkening law and fit directly for u_1 and u_2 assuming large uniform priors ($U[-3,3]$) following Coulombe et al. (2024). For the first visit, we consider a quadratic trend for the systematics model. We also include in the fit a Matérn 3/2 Gaussian Process using the `celerite` python (Foreman-Mackey et al. 2017) to remove higher-frequency trends that are not corrected by our systematics model. The timescale and amplitude of the GP model are kept free assuming large uninformative uniform priors in log-space. As for the second visit, we cut the first 2.1 hours of the TSO and consider solely a linear slope for the systematics model. The transit light curves are then modelled in ExoTEP using the `batman` (Kreidberg 2015) python package, and we explore the parameter space using and the Markov chain Monte Carlo (MCMC) sampler `emcee` (Foreman-Mackey et al. 2013). We run the MCMC for 10,000 steps and discard the first 6,000 steps as burn-in. The same procedure is repeated for the spectroscopic light curves (assuming the same systematics model and GP for each visit), where we have fixed the orbital parameters of TRAPPIST-1c to the best-fit values from the white-light curve of the first visit ($a/R_* = 28.55$, $b = 0.112$). The light curves are fit using 100 and 30 equal-pixel bins for the first and second spectral orders, respectively. The resulting spectra, binned to a fixed resolving power of $R = 25$, are shown in Figure 6.

B. ADDITIONAL TABLES

Table 1 contains the best-fitting white light curve parameters for both NIRISS/SOSS visits. The orbital parameters (a/R_* , b) are consistent with each other, and with previous literature (e.g., Agol et al. 2021).

Table 2 has the `exoTEDRF` transmission spectrum used in this work.

³ <https://jwst-docs.stsci.edu/>

Table 1. Best-fitting exoTDRF white light transit parameters

Parameter	Value		
	Visit 1	Visit 2	Weighted Average
T0 [BJD]	2459881.401521 ^{+0.000032} _{-0.000031}	2460249.515096 ^{+0.000034} _{-0.000033}	-
R _p /R _* ,O1	0.08452 ^{+0.00076} _{-0.00083}	0.08372 ^{+0.00102} _{-0.00145}	0.08432 ± 0.00072
R _p /R _* ,O2	0.08421 ^{+0.00235} _{-0.00226}	0.08405 ^{+0.00251} _{-0.00225}	0.08414 ± 0.00172
b	0.133 ^{+0.083} _{-0.098}	0.136 ^{+0.036} _{-0.028}	0.136 ± 0.034
a/R _*	28.31 ^{+0.43} _{-0.26}	28.12 ^{+0.49} _{-0.54}	28.24 ± 0.34
q ₁ ,O1	0.358 ^{+0.096} _{-0.113}	0.473 ^{+0.099} _{-0.128}	0.408 ± 0.085
q ₂ ,O1	0.339 ^{+0.109} _{-0.141}	0.163 ^{+0.095} _{-0.133}	0.246 ± 0.097
q ₁ ,O2	0.374 ^{+0.162} _{-0.247}	0.642 ^{+0.142} _{-0.177}	0.551 ± 0.144
q ₂ ,O2	0.516 ^{+0.296} _{-0.300}	0.769 ^{+0.220} _{-0.156}	0.681 ± 0.177

Notes: For each visit, R_p/R_{*} and the limb darkening parameters (q₁ and q₂) were fit separately for each order. All other parameters were jointly fit to both.

Table 2. exoTDRF transmission spectrum of TRAPPIST-1 c used in this work

Wavelength (μm)	Wavelength Error (μm)	Transit Depth (visit 1) (ppm)	Transit Depth (visit 2) (ppm)
0.72	0.12	6050.99 ± 473.23	6982.25 ± 418.63
0.90	0.04	6585.89 ± 111.83	6757.96 ± 135.93
0.98	0.04	6772.63 ± 91.97	6808.19 ± 128.63
1.05	0.04	6881.03 ± 71.42	6960.16 ± 89.30
1.12	0.04	6820.05 ± 69.73	6849.88 ± 64.50
1.20	0.04	6699.58 ± 63.55	6907.84 ± 80.39
1.28	0.04	6694.65 ± 64.58	6697.34 ± 90.68
1.35	0.04	6971.35 ± 60.31	7023.65 ± 58.31
1.43	0.04	6886.42 ± 76.10	7001.35 ± 76.95
1.51	0.04	6847.72 ± 84.78	6937.97 ± 88.64
1.59	0.04	6789.90 ± 76.61	6902.63 ± 90.38
1.66	0.04	6895.75 ± 74.07	7088.25 ± 92.70
1.74	0.04	6914.99 ± 90.90	6899.64 ± 100.01
1.82	0.04	7006.82 ± 97.16	7136.91 ± 144.17
1.90	0.04	6804.84 ± 126.15	6967.40 ± 122.15
1.98	0.04	7032.96 ± 118.65	7127.79 ± 126.21
2.06	0.04	6796.19 ± 132.58	6970.70 ± 136.08
2.14	0.04	6842.86 ± 136.57	6972.46 ± 134.27
2.21	0.04	7010.63 ± 135.26	6977.26 ± 147.22
2.29	0.04	6919.63 ± 128.65	6890.04 ± 155.09
2.37	0.04	6707.69 ± 153.51	6972.92 ± 152.57
2.45	0.04	6643.73 ± 180.88	6821.97 ± 202.91
2.53	0.04	6770.44 ± 232.33	7296.84 ± 270.63
2.61	0.04	6837.59 ± 233.79	6966.78 ± 293.63
2.69	0.04	6183.53 ± 235.11	6961.30 ± 273.61
2.77	0.04	6589.56 ± 270.29	6630.95 ± 311.46

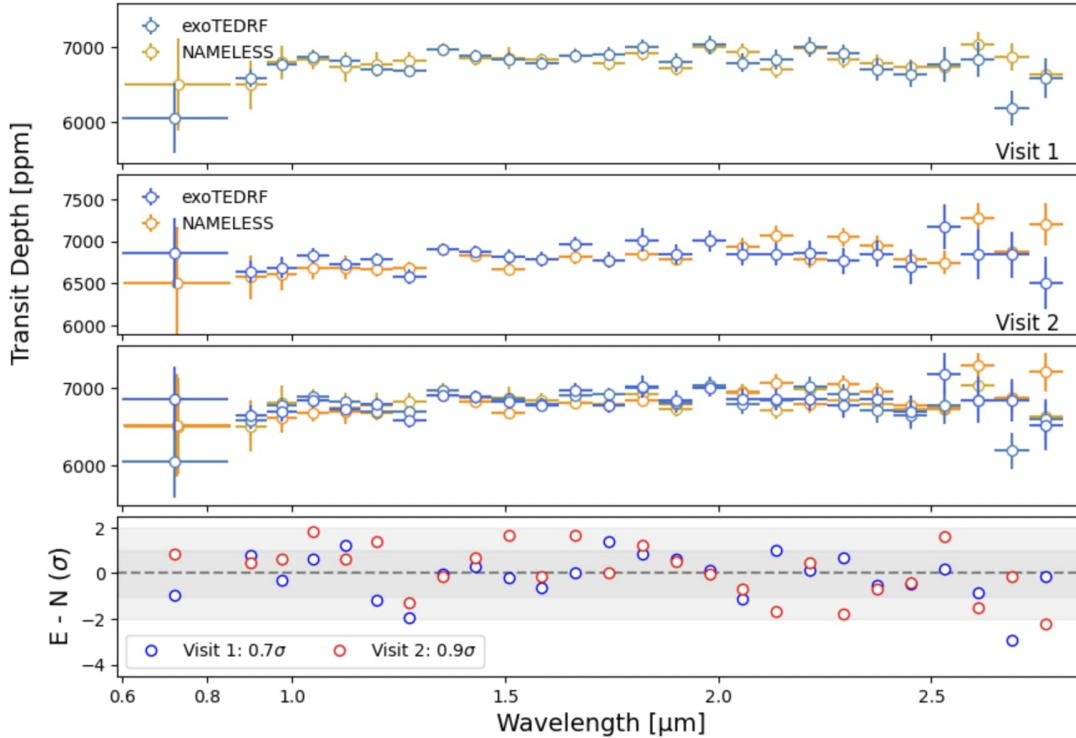


Figure 6. Comparison of transmission spectra from the `exoTDRF` and `NAMELESS` pipelines. *Top panel:* Spectrum comparison for visit 1. *Second panel:* Same as top but for visit 2. *Third panel:* All four spectra from both pipeline and for both visits overplotted to show consistency. *Bottom panel:* Differences between spectra from each pipeline for visit 1 (blue) and visit 2 (red) divided by the error bar on each transit depth. The `exoTDRF` and `NAMELESS` spectra are consistent to within 0.7σ on average for visit 1 and 0.9σ for visit 2. Note that a ~ 122 ppm offset between the visit 1 and visit 2 spectra has been corrected here.

REFERENCES

- Agol, E., Dorn, C., Grimm, S. L., et al. 2021, *Planet. Sci. J.*, 2, 1, doi: [10.3847/PSJ/abd022](https://doi.org/10.3847/PSJ/abd022)
- Albert, L., Lafrenière, D., René, D., et al. 2023, *PASP*, 135, 075001, doi: [10.1088/1538-3873/acd7a3](https://doi.org/10.1088/1538-3873/acd7a3)
- Astropy Collaboration, Robitaille, T. P., Tollerud, E. J., et al. 2013, *A&A*, 558, A33, doi: [10.1051/0004-6361/201322068](https://doi.org/10.1051/0004-6361/201322068)
- Astropy Collaboration, Price-Whelan, A. M., Sipőcz, B. M., et al. 2018, *AJ*, 156, 123, doi: [10.3847/1538-3881/aabc4f](https://doi.org/10.3847/1538-3881/aabc4f)
- Benneke, B. 2015, *Strict Upper Limits on the Carbon-to-Oxygen Ratios of Eight Hot Jupiters from Self-Consistent Atmospheric Retrieval*, arXiv. <http://arxiv.org/abs/1504.07655>
- Benneke, B., & Seager, S. 2012, *ApJ*, 753, 100, doi: [10.1088/0004-637X/753/2/100](https://doi.org/10.1088/0004-637X/753/2/100)
- . 2013, *ApJ*, 778, 153, doi: [10.1088/0004-637X/778/2/153](https://doi.org/10.1088/0004-637X/778/2/153)
- Benneke, B., Knutson, H. A., Lothringer, J., et al. 2019a, *Nat Astron*, 3, 813, doi: [10.1038/s41550-019-0800-5](https://doi.org/10.1038/s41550-019-0800-5)
- Benneke, B., Wong, I., Piaulet, C., et al. 2019b, *ApJL*, 887, L14, doi: [10.3847/2041-8213/ab59dc](https://doi.org/10.3847/2041-8213/ab59dc)
- Benneke, B., Roy, P.-A., Coulombe, L.-P., et al. 2024, *JWST Reveals CH₄, CO₂, and H₂O in a Metal-rich Miscible Atmosphere on a Two-Earth-Radius Exoplanet*, arXiv. <http://arxiv.org/abs/2403.03325>
- Bolmont, E., Selsis, F., Owen, J. E., et al. 2017, *Mon. Not. R. Astron. Soc.*, 464, 3728, doi: [10.1093/mnras/stw2578](https://doi.org/10.1093/mnras/stw2578)
- Buchner, J. 2016, *Stat Comput*, 26, 383, doi: [10.1007/s11222-014-9512-y](https://doi.org/10.1007/s11222-014-9512-y)
- Burgasser, A. J., & Mamajek, E. E. 2017, *The Astrophysical Journal*, 845, 110, doi: [10.3847/1538-4357/aa7fea](https://doi.org/10.3847/1538-4357/aa7fea)
- Bushouse, H., Eisenhamer, J., Dencheva, N., et al. 2022, *JWST Calibration Pipeline, 1.7.0*, Zenodo, doi: [10.5281/zenodo.7038885](https://doi.org/10.5281/zenodo.7038885)
- Cadieux, C., Doyon, R., MacDonald, R. J., et al. 2024, *ApJL*, 970, L2, doi: [10.3847/2041-8213/ad5afa](https://doi.org/10.3847/2041-8213/ad5afa)
- Charnay, B., Forget, F., Tobie, G., Sotin, C., & Wordsworth, R. 2014, *Icarus*, 241, 269–279, doi: [10.1016/j.icarus.2014.07.009](https://doi.org/10.1016/j.icarus.2014.07.009)

- Coulombe, L.-P., Roy, P.-A., & Benneke, B. 2024, arXiv e-prints, arXiv:2409.03812, doi: [10.48550/arXiv.2409.03812](https://doi.org/10.48550/arXiv.2409.03812)
- Coulombe, L.-P., Benneke, B., Challener, R., et al. 2023, *Nature*, 620, 292, doi: [10.1038/s41586-023-06230-1](https://doi.org/10.1038/s41586-023-06230-1)
- Damiano, M., Bello-Arufe, A., Yang, J., & Hu, R. 2024, *The Astrophysical Journal Letters*, 968, L22, doi: [10.3847/2041-8213/ad5204](https://doi.org/10.3847/2041-8213/ad5204)
- Darveau-Bernier, A., Albert, L., Talens, G. J., et al. 2022, *PASP*, 134, 094502, doi: [10.1088/1538-3873/ac8a77](https://doi.org/10.1088/1538-3873/ac8a77)
- De Wit, J., Wakeford, H. R., Gillon, M., et al. 2016, *Nature*, 537, 69, doi: [10.1038/nature18641](https://doi.org/10.1038/nature18641)
- Doyon, R., Willott, C. J., Hutchings, J. B., et al. 2023, *PASP*, 135, 098001, doi: [10.1088/1538-3873/acd41b](https://doi.org/10.1088/1538-3873/acd41b)
- Ducrot, E., Gillon, M., Delrez, L., et al. 2020, *Astronomy & Astrophysics*, 640, A112, doi: [10.1051/0004-6361/201937392](https://doi.org/10.1051/0004-6361/201937392)
- Espinoza, N., Kossakowski, D., & Brahm, R. 2019, *Monthly Notices of the Royal Astronomical Society*, 490, 2262, doi: [10.1093/mnras/stz2688](https://doi.org/10.1093/mnras/stz2688)
- Feinstein, A. D., Radica, M., Welbanks, L., et al. 2023, *Nature*, 614, 670, doi: [10.1038/s41586-022-05674-1](https://doi.org/10.1038/s41586-022-05674-1)
- Foreman-Mackey, D., Agol, E., Ambikasaran, S., & Angus, R. 2017, *AJ*, 154, 220, doi: [10.3847/1538-3881/aa9332](https://doi.org/10.3847/1538-3881/aa9332)
- Foreman-Mackey, D., Hogg, D. W., Lang, D., & Goodman, J. 2013, *Publications of the Astronomical Society of the Pacific*, 125, 306, doi: [10.1086/670067](https://doi.org/10.1086/670067)
- Fournier-Tondreau, M., MacDonald, R. J., Radica, M., et al. 2024, *Monthly Notices of the Royal Astronomical Society*, 528, 3354, doi: [10.1093/mnras/stad3813](https://doi.org/10.1093/mnras/stad3813)
- Gillon, M., Jehin, E., Lederer, S. M., et al. 2016, *Nature*, 533, 221, doi: [10.1038/nature17448](https://doi.org/10.1038/nature17448)
- Greene, T. P., Bell, T. J., Ducrot, E., et al. 2023, *Nature*, 618, 39, doi: [10.1038/s41586-023-05951-7](https://doi.org/10.1038/s41586-023-05951-7)
- Grenfell, J. L. 2020, *Habitability, Role of the Atmosphere* (Berlin, Heidelberg: Springer Berlin Heidelberg), 1–6, doi: [10.1007/978-3-642-27833-4_5098-2](https://doi.org/10.1007/978-3-642-27833-4_5098-2)
- Harris, C. R., Millman, K. J., van der Walt, S. J., et al. 2020, *Nature*, 585, 357, doi: [10.1038/s41586-020-2649-2](https://doi.org/10.1038/s41586-020-2649-2)
- Holmberg, M., & Madhusudhan, N. 2023, *Monthly Notices of the Royal Astronomical Society*, 524, 377, doi: [10.1093/mnras/stad1580](https://doi.org/10.1093/mnras/stad1580)
- Hori, Y., & Ogihara, M. 2020, *ApJ*, 889, 77, doi: [10.3847/1538-4357/ab6168](https://doi.org/10.3847/1538-4357/ab6168)
- Howard, W. S., Kowalski, A. F., Flagge, L., et al. 2023, *ApJ*, 959, 64, doi: [10.3847/1538-4357/acfe75](https://doi.org/10.3847/1538-4357/acfe75)
- Hu, R., Gaillard, F., & Kite, E. S. 2023, *ApJL*, 948, L20, doi: [10.3847/2041-8213/acd0b4](https://doi.org/10.3847/2041-8213/acd0b4)
- Hunter, J. D. 2007, *Computing in Science & Engineering*, 9, 90, doi: [10.1109/MCSE.2007.55](https://doi.org/10.1109/MCSE.2007.55)
- Husser, T.-O., Wende-von Berg, S., Dreizler, S., et al. 2013, *A&A*, 553, A6, doi: [10.1051/0004-6361/201219058](https://doi.org/10.1051/0004-6361/201219058)
- Ih, J., Kempton, E. M.-R., Whittaker, E. A., & Lessard, M. 2023, *ApJL*, 952, L4, doi: [10.3847/2041-8213/ace03b](https://doi.org/10.3847/2041-8213/ace03b)
- Kallinger, T., De Ridder, J., Hekker, S., et al. 2014, *A&A*, 570, A41, doi: [10.1051/0004-6361/201424313](https://doi.org/10.1051/0004-6361/201424313)
- Kasai, Y., Dupuy, E., Saito, R., et al. 2011, *Atmospheric Chemistry and Physics*, 11, 8607, doi: [10.5194/acp-11-8607-2011](https://doi.org/10.5194/acp-11-8607-2011)
- Kelsey, V., Riley, S., & Minschwaner, K. 2022, *Atmospheric Measurement Techniques*, 15, 1563, doi: [10.5194/amt-15-1563-2022](https://doi.org/10.5194/amt-15-1563-2022)
- Kipping, D. M. 2013, *Monthly Notices of the Royal Astronomical Society*, 435, 2152, doi: [10.1093/mnras/stt1435](https://doi.org/10.1093/mnras/stt1435)
- Kirk, J., Stevenson, K. B., Fu, G., et al. 2024, *AJ*, 167, 90, doi: [10.3847/1538-3881/ad19df](https://doi.org/10.3847/1538-3881/ad19df)
- Kreidberg, L. 2015, *Publications of the Astronomical Society of the Pacific*, 127, 1161, doi: [10.1086/683602](https://doi.org/10.1086/683602)
- Kreidberg, L., Koll, D. D. B., Morley, C., et al. 2019, *Nature*, 573, 87, doi: [10.1038/s41586-019-1497-4](https://doi.org/10.1038/s41586-019-1497-4)
- Krissansen-Totton, J. 2023, *ApJL*, 951, L39, doi: [10.3847/2041-8213/acdc26](https://doi.org/10.3847/2041-8213/acdc26)
- Krissansen-Totton, J., & Fortney, J. J. 2022, *ApJ*, 933, 115, doi: [10.3847/1538-4357/ac69cb](https://doi.org/10.3847/1538-4357/ac69cb)
- Libby-Roberts, J. E., Berta-Thompson, Z. K., Diamond-Lowe, H., et al. 2022, *The Astronomical Journal*, 164, 59, doi: [10.3847/1538-3881/ac75de](https://doi.org/10.3847/1538-3881/ac75de)
- Lim, O., Benneke, B., Doyon, R., et al. 2023, *ApJL*, 955, L22, doi: [10.3847/2041-8213/acf7c4](https://doi.org/10.3847/2041-8213/acf7c4)
- Lloyd, R. O. P., Shkolnik, E. L., Schneider, A. C., et al. 2021, *The Astrophysical Journal*, 907, 91, doi: [10.3847/1538-4357/abd0f0](https://doi.org/10.3847/1538-4357/abd0f0)
- Luger, R., & Barnes, R. 2015, *Astrobiology*, 15, 119, doi: [10.1089/ast.2014.1231](https://doi.org/10.1089/ast.2014.1231)
- Luger, R., Sestovic, M., Kruse, E., et al. 2017, *Nature Astronomy*, 1, 0129, doi: [10.1038/s41550-017-0129](https://doi.org/10.1038/s41550-017-0129)
- Lustig-Yaeger, J., Fu, G., May, E. M., et al. 2023, *Nat Astron*, 7, 1317, doi: [10.1038/s41550-023-02064-z](https://doi.org/10.1038/s41550-023-02064-z)
- Mansfield, M. W., Xue, Q., Zhang, M., et al. 2024, *No Thick Atmosphere on the Terrestrial Exoplanet Gl 486b*, arXiv. <http://arxiv.org/abs/2408.15123>
- May, E. M., MacDonald, R. J., Bennett, K. A., et al. 2023, *ApJL*, 959, L9, doi: [10.3847/2041-8213/ad054f](https://doi.org/10.3847/2041-8213/ad054f)
- Moran, S. E., Stevenson, K. B., Sing, D. K., et al. 2023, *ApJL*, 948, L11, doi: [10.3847/2041-8213/accb9c](https://doi.org/10.3847/2041-8213/accb9c)
- Peacock, S., Barman, T., Shkolnik, E. L., Hauschildt, P. H., & Baron, E. 2019, *The Astrophysical Journal*, 871, 235, doi: [10.3847/1538-4357/aaf891](https://doi.org/10.3847/1538-4357/aaf891)

- Pelletier, S., Benneke, B., Darveau-Bernier, A., et al. 2021, *AJ*, 162, 73, doi: [10.3847/1538-3881/ac0428](https://doi.org/10.3847/1538-3881/ac0428)
- Pereira, F., Campante, T. L., Cunha, M. S., et al. 2019, *Monthly Notices of the Royal Astronomical Society*, 489, 5764, doi: [10.1093/mnras/stz2405](https://doi.org/10.1093/mnras/stz2405)
- Pérez, F., & Granger, B. E. 2007, *Computing in Science and Engineering*, 9, 21, doi: [10.1109/MCSE.2007.53](https://doi.org/10.1109/MCSE.2007.53)
- Piaulet, C., Benneke, B., Almenara, J. M., et al. 2023, *Nature Astronomy*, 7, 206, doi: [10.1038/s41550-022-01835-4](https://doi.org/10.1038/s41550-022-01835-4)
- Piaulet-Ghorayeb, C. 2024, First release of stellar contamination modeling and retrieval code, 1.0.0, Zenodo, doi: [10.5281/zenodo.13153252](https://doi.org/10.5281/zenodo.13153252)
- Pizzolato, N., Maggio, A., Micela, G., Sciortino, S., & Ventura, P. 2003, *Astronomy & Astrophysics*, 397, 147, doi: [10.1051/0004-6361:20021560](https://doi.org/10.1051/0004-6361:20021560)
- Rackham, B. V., Apai, D., & Giampapa, M. S. 2018, *ApJ*, 853, 122, doi: [10.3847/1538-4357/aaa08c](https://doi.org/10.3847/1538-4357/aaa08c)
- . 2019, *AJ*, 157, 96, doi: [10.3847/1538-3881/aaf892](https://doi.org/10.3847/1538-3881/aaf892)
- Rackham, B. V., Espinoza, N., Berdyugina, S. V., et al. 2023, *RAS Techniques and Instruments*, 2, 148, doi: [10.1093/rasti/rzad009](https://doi.org/10.1093/rasti/rzad009)
- Radica, M. 2024, *JOSS*, 9, 6898, doi: [10.21105/joss.06898](https://doi.org/10.21105/joss.06898)
- Radica, M. 2024, *radicamc/exoUPRF: v1.0.1, v1.0.1*, Zenodo, doi: [10.5281/zenodo.12628066](https://doi.org/10.5281/zenodo.12628066)
- Radica, M., Albert, L., Taylor, J., et al. 2022, *PASP*, 134, 104502, doi: [10.1088/1538-3873/ac9430](https://doi.org/10.1088/1538-3873/ac9430)
- Radica, M., Welbanks, L., Espinoza, N., et al. 2023, *Monthly Notices of the Royal Astronomical Society*, 524, 835, doi: [10.1093/mnras/stad1762](https://doi.org/10.1093/mnras/stad1762)
- Radica, M., Coulombe, L.-P., Taylor, J., et al. 2024, *ApJL*, 962, L20, doi: [10.3847/2041-8213/ad20e4](https://doi.org/10.3847/2041-8213/ad20e4)
- Skilling, J. 2004, in *American Institute of Physics Conference Series*, Vol. 735, *Bayesian Inference and Maximum Entropy Methods in Science and Engineering: 24th International Workshop on Bayesian Inference and Maximum Entropy Methods in Science and Engineering*, ed. R. Fischer, R. Preuss, & U. V. Toussaint (AIP), 395–405, doi: [10.1063/1.1835238](https://doi.org/10.1063/1.1835238)
- Skilling, J. 2006, *Bayesian Anal.*, 1, doi: [10.1214/06-BA127](https://doi.org/10.1214/06-BA127)
- Taylor, J., Radica, M., Welbanks, L., et al. 2023, *Monthly Notices of the Royal Astronomical Society*, 524, 817, doi: [10.1093/mnras/stad1547](https://doi.org/10.1093/mnras/stad1547)
- Townsend, R., & Lopez, A. 2023, *Journal of Open Source Software*, 8, 4602, doi: [10.21105/joss.04602](https://doi.org/10.21105/joss.04602)
- TRAPPIST-1 JWST Community Initiative, De Wit, J., Doyon, R., et al. 2024, *Nat Astron*, 8, 810, doi: [10.1038/s41550-024-02298-5](https://doi.org/10.1038/s41550-024-02298-5)
- Turbet, M., Bolmont, E., Bourrier, V., et al. 2020, *SSRv*, 216, 100, doi: [10.1007/s11214-020-00719-1](https://doi.org/10.1007/s11214-020-00719-1)
- Turbet, M., Bolmont, E., Leconte, J., et al. 2018, *A&A*, 612, A86, doi: [10.1051/0004-6361/201731620](https://doi.org/10.1051/0004-6361/201731620)
- Turbet, M., Fauchez, T. J., Leconte, J., et al. 2023, *A&A*, 679, A126, doi: [10.1051/0004-6361/202347539](https://doi.org/10.1051/0004-6361/202347539)
- Van Looveren, G., Güdel, M., Boro Saikia, S., & Kislyakova, K. 2024, *A&A*, 683, A153, doi: [10.1051/0004-6361/202348079](https://doi.org/10.1051/0004-6361/202348079)
- Virtanen, P., Gommers, R., Oliphant, T. E., et al. 2020, *Nature Methods*, 17, 261, doi: [10.1038/s41592-019-0686-2](https://doi.org/10.1038/s41592-019-0686-2)
- Wakeford, H. R., Lewis, N. K., Fowler, J., et al. 2019, *AJ*, 157, 11, doi: [10.3847/1538-3881/aaf04d](https://doi.org/10.3847/1538-3881/aaf04d)
- Wheatley, P. J., Louden, T., Bourrier, V., Ehrenreich, D., & Gillon, M. 2017, *Monthly Notices of the Royal Astronomical Society*, 465, L74, doi: [10.1093/mnrasl/slw192](https://doi.org/10.1093/mnrasl/slw192)
- Wordsworth, R. D., & Pierrehumbert, R. T. 2013, *The Astrophysical Journal*, 778, 154, doi: [10.1088/0004-637X/778/2/154](https://doi.org/10.1088/0004-637X/778/2/154)
- Wright, N. J., Drake, J. J., Mamajek, E. E., & Henry, G. W. 2011, *The Astrophysical Journal*, 743, 48, doi: [10.1088/0004-637X/743/1/48](https://doi.org/10.1088/0004-637X/743/1/48)
- Xue, Q., Bean, J. L., Zhang, M., et al. 2024, *JWST Thermal Emission of the Terrestrial Exoplanet GJ 1132b*, arXiv. <http://arxiv.org/abs/2408.13340>
- Zahnle, K. J., & Catling, D. C. 2017, *ApJ*, 843, 122, doi: [10.3847/1538-4357/aa7846](https://doi.org/10.3847/1538-4357/aa7846)
- Zhang, M., Hu, R., Inglis, J., et al. 2024, *ApJL*, 961, L44, doi: [10.3847/2041-8213/ad1a07](https://doi.org/10.3847/2041-8213/ad1a07)
- Zieba, S., Kreidberg, L., Ducrot, E., et al. 2023, *Nature*, 620, 746, doi: [10.1038/s41586-023-06232-z](https://doi.org/10.1038/s41586-023-06232-z)